ACS APPLIED MATERIALS & INTERFACES

Research Article

Cite This: ACS Appl. Mater. Interfaces 2019, 11, 43223−43234

www.acsami.org

Inhibiting Charge Recombination in *cis*-Ru(NCS)$_2$ Diimine Sensitizers with Aromatic Substituents

Andressa V. Müller,[†,‡] Kleber T. de Oliveira,[§] Gerald J. Meyer,[*,‡] and André S. Polo[*,†]

[†]Centro de Ciências Naturais e Humanas, Universidade Federal do ABC—UFABC, Av. dos Estados, 5001, 09210-580 Santo André, São Paulo, Brazil

[‡]Department of Chemistry, University of North Carolina at Chapel Hill, Chapel Hill, North Carolina 27599, United States

[§]Departamento de Química, Universidade Federal de São Carlos—UFSCar, Rodovia Washington Luís, km 235, 13565-905 São Carlos, São Paulo, Brazil

ABSTRACT: A series of *cis*-[Ru(LL)(dcbH$_2$)(NCS)$_2$] compounds, where dcbH$_2$ = 2,2′-bipyridine-4,4′-dicarboxylic acid and LL = 1,10-phenanthroline (Ru(phen)), 4,7-dipyrrole-1,10-phenanthroline (Ru(pyr)), 4,7-diindole-1,10-phenanthroline (Ru(ind)), or 4,7-dicarbazole-1,10-phenanthroline (Ru(cbz)), was investigated for application as sensitizers in mesoporous TiO$_2$ dye-sensitized solar cells (DSSCs). A systematic increase in the number of rings of the aromatic substituents at the 4,7-positions of the 1,10-phenanthroline allowed tuning of the molecular size of the sensitizers and the energy stored in the excited state while maintaining the same ground-state Ru$^{3+/2+}$ reduction potentials. These small structural changes had a significant influence on the rates and/or efficiencies of electron injection, back-electron transfer, recombination to oxidized mediators, lateral self-exchange electron transfer, and regeneration through iodide oxidation that were reflected in distinct photoelectrochemical performance of full operating DSSCs. The global efficiencies, open-circuit voltages, and short-circuit current densities of the DSSCs consistently followed the trend Ru(pyr) < Ru(ind) < Ru(phen) < Ru(cbz), and the most optimal performance of Ru(cbz) was ascribed to dramatically slower recombination to the oxidized redox mediators. Transient photovoltage and transient absorption experiments both revealed significantly slower recombination as the size of the aromatic substituents increased with Ru(cbz) providing the most promising behavior for application in dye sensitization.

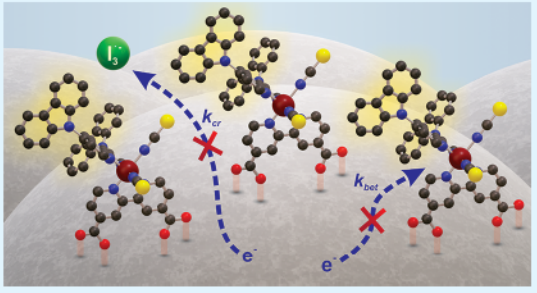

KEYWORDS: *DSSC, recombination, hole-hopping, regeneration, electron transfer, steric effects*

INTRODUCTION

Understanding and controlling the forward and backward electron transfer processes involved in the light-initiated energy conversion are the key points for the development of highly efficient dye-sensitized solar cells (DSSCs). After dye excitation, electron injection into the semiconductor oxide must be faster than excited state relaxation to the ground state. Additionally, collection of the injected electron at the back-contact and the regeneration of the oxidized dye must be fast enough to avoid energy losses due to electron transfer to the oxidized dye molecules or to the electrolyte.[1]

One possibility to tune the rates of these electron transfer reactions is through the molecular engineering of the dye sensitizer. It has been extensively shown that modifications in the structure of the polypyridyl ancillary ligands, LL, in *cis*-[Ru(LL)(dcbH$_2$)(NCS)$_2$] dyes, dcbH$_2$ = 2,2′-bipyridine-4,4′-dicarboxylic acid, change the electron transfer dynamics and, ultimately, the efficiencies of the DSSCs. The presence of electron donating or withdrawing groups in these ligands may change the electronic energy levels of the compounds, the recombination and regeneration rates, and also the injection quantum yields.[2−4] More recently, evidence that the molecular size of the sensitizer plays an important role in the rates of lateral self-exchange electron transfer and consequently affects the dynamics of back-electron transfer has been provided.[3,5−8]

In this study, four *cis*-[Ru(LL)(dcbH$_2$)(NCS)$_2$] dye sensitizers, LL = 1,10-phenanthroline (Ru(phen)), 4,7-dipyrrole-1,10-phenanthroline (Ru(pyr)), 4,7-diindole-1,10-phenanthroline (Ru(ind)), or 4,7-dicarbazole-1,10-phenanthroline (Ru(cbz)), Figure 1, were investigated. A systematic increase in the number of aromatic rings at the 4,7 positions of 1,10-phenanthroline allowed tuning of the molecular size of the sensitizers while maintaining the same ground-state Ru$^{3+/2+}$ reduction potential for all of the complexes. These small structural changes resulted in significant effects in the rates and/or efficiencies of electron injection, back-electron transfer, recombination to oxidized mediators, lateral self-exchange electron transfer, and regeneration of the oxidized dyes that were reflected in distinct photoelectrochemical performance of full operating DSSCs. The results herein presented provided useful insights into the role of steric effects on the electron

Received: August 27, 2019
Accepted: October 24, 2019
Published: October 24, 2019

DOI: 10.1021/acsami.9b15448
ACS Appl. Mater. Interfaces 2019, 11, 43223−43234

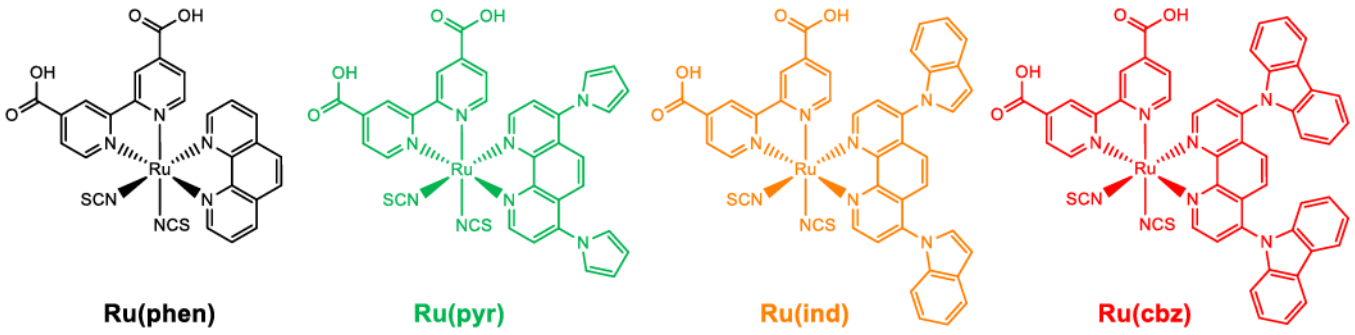

Figure 1. Molecular structures and abbreviations of the *cis*-[Ru(LL)($dcbH_2$)$(NCS)_2$] dyes investigated in this study.

transfer dynamics that drive energy conversion in these devices.

EXPERIMENTAL SECTION

Materials. The following materials and reagents were used as received from the indicated commercial suppliers: *N*,*N*′-dimethylformamide (DMF; Vetec, ≥99.8%), methanol (Synth, 99.8%), ethanol (Merck, LiChrosolv, ≥99.9%), acetonitrile (Sigma-Aldrich, HPLC grade, ≥99.9% or Burdick & Jackson, spectrophotometric grade), tetrahydrofuran (THF; Sigma-Aldrich, HPLC grade, ≥99.9%), toluene (Synth, 99.5%), ethyl acetate (Synth, 99.5%), ethyl ether (Synth, 98.0%), isopropanol (Synth, 99.5%), valeronitrile (Aldrich, 99.5%), DMF-d_7 (Aldrich, ≥99.5%), D_2O (Aldrich, 99.96%), NaOD (Aldrich, 99.5%), HCl (Synth, 36.5%), H_2SO_4 (Merck, 95−97%), HNO_3 (Synth, 65.0%), NaOH (Sigma-Aldrich, > 98%), methanolic solution of tetrabutylammonium hydroxide (TBAOH; Sigma-Aldrich, 1 mol L^{-1}), [Ru(*p*-cymene)Cl_2]$_2$ (Strem, 98%), 4,4′-dimethyl-2,2′-bypyridine (Aldrich, 99%), 1,10-phenanthroline (phen; Strem, 99%), 4,7-dichloro-1,10-phenanthroline (E-novation, 97%), indole (Aldrich, ≥99%), carbazole (Aldrich, ≥95%), potassium *tert*-butoxide (Aldrich, ≥98%), $Na_2Cr_2O_7$ (Synth, 99.5%), Na_2SO_4 (Synth, anhydrous, 99,0%), NaH (Aldrich, 60% dispersion in mineral oil), NaNCS (Merck, 98.5%), H_2PtCl_6 (Acros, 99.9%), I_2 (Sigma-Aldrich, ≥99.9%), guanidine thiocyanate (Sigma-Aldrich, ≥97%), 4-*tert*-butylpyridine (Aldrich, 96%), 1-butyl-3-methylimidazolium iodide (Aldrich, 98%), tetra-*n*-butylammonium hexafluorophosphate (TBAPF_6; Fluka, ≥99.0%), tetra-*n*-butylammonium iodide (TBAI; Sigma-Aldrich, ≥99.0%), ferrocene (Aldrich, 98%), silica gel (Sigma-Aldrich, ≥98%), Sephadex LH-20 (Sigma), transparent 20 nm TiO_2 anatase nanoparticles paste (18NR-T, Dyesol), titanium(IV) isopropoxide (Sigma-Aldrich, 97%), In_2O_3:Sn (ITO) nanoparticles (Evonik Industries, TC8 DE, 20 wt % dispersion in ethanol), Carbowax (Sigma-Aldrich), hydroxypropyl cellulose (Sigma-Aldrich, average M_W = 80 000, 20 mesh particle size), fluorine-doped SnO_2-coated glass (FTO; Aldrich, 3.2 mm thick, 8 Ω $\square^{-1}$ or Hartford Glass Co., Inc., 2.3 mm thick, 15 Ω $\square^{-1}$), glass coverslip (Microscope Cover Glass 12-542-B, Fischer Scientific), low temperature sealant - Surlyn (30 mm - Dyesol), and argon gas (Airgas, >99.998%). Pyrrole (Aldrich, 98%) was freshly distilled using a Vigreaux column prior to use.

Syntheses. *2,2′-Bipyridine-4,4′-dicarboxylic Acid.* The ligand 2,2′-bipyridine-4,4′-dicarboxylic acid ($dcbH_2$) was synthesized according to the procedure previously reported in the literature.[9] Yield = 89%. (Anal. Calcd for $C_{12}H_8N_2O_4$: C, 59.02; H, 3.30; N, 11.47%. Found: C, 58.67; H, 3.38; N, 11.12%. NMR ^{1}H (D_2O/NaOD, 500 MHz, δ/ppm): 8.61 (d, 2H, J = 4.9 Hz); 8.19 (s, 2H); 7.73 (d, 2H, J = 4.9 Hz)).

4,7-Substituted-1,10-phenanthrolines. The ligands pyr and ind were prepared by adding 4.5 mmol of pyrrole (0.32 mL) or indole (0.53 g) and 10 mL of THF to a 50 mL round-bottom flask under argon atmosphere. Then, 4.0 mmol of NaH (0.19 g) was added, and the mixture was heated to reflux. After 2 h, the heating was interrupted, and after the flask reached room temperature, 1.0 mmol of 4,7-dichloro-1,10-phenanthroline (0.25 g) was added. The mixture was then heated under reflux and argon atmosphere for 48 h. The reaction was quenched by adding water (25 mL), and the products were extracted with toluene and ethyl acetate. The organic layers were dried over anhydrous sodium sulfate, and the solvent was distilled off under reduced pressure. To the solid, 10 mL of ethyl ether was added, and the suspension was sonicated for 1 min, stirred for 10 min, and filtered. The resulting solid was rinsed with 5 mL of ethyl ether and dried in a desiccator under vacuum with silica gel.

pyr (Yield = 73%. Anal. Calcd for $C_{20}H_{14}N_4$: C, 77.40; H, 4.55; N, 18.05%; Found: C, 77.60; H, 4,52; N, 17.98%. NMR ^{1}H ($CDCl_3$, 500 MHz, δ/ppm): 9.24 (d, 2H, J = 4.7 Hz); 8.00 (s, 2H); 7.59 (d, 2H, J = 4.7 Hz); 7.09 (t, 4H, J = 2.1 Hz); 6.48 (t, 4H, J = 2.1 Hz)).

ind (Yield = 59%. Anal. Calcd for $C_{28}H_{18}N_4$: C, 81.93; H, 4.42; N, 13.65%; Found: C, 81.78; H, 4.28; N, 13.31%. NMR ^{1}H ($CDCl_3$, 500 MHz, δ/ppm): 9.31 (d, 2H, J = 4.7 Hz); 7.83 (d, 2H, J = 4.7 Hz); 7.74 (m, 2H); 7.56 (s, 2H); 7.54 (d, 2H, J = 3.3 Hz); 7.19 (m, 6H); 6.86 (d, 2H, J = 3.4 Hz)).

The ligand cbz was prepared according to the procedure previously reported.[9,10] Yield = 54% (Anal. Calcd for $C_{36}H_{22}N_4$: C, 84.68; H, 4.34; N, 10.97%; Found: C, 84.45; H, 4.54; N, 11.17%. NMR ^{1}H ($CDCl_3$, 500 MHz, δ/ppm): 9.54 (d, 2H, J = 4.7 Hz); 8.14 (m, 4H); 7,91 (d, 2H, J = 4.8 Hz); 7.41 (s, 2H); 7.32 (m, 8H); 7.07 (m, 4H)).

cis-[Ru(LL)(dcbH$_2$)(NCS)$_2$] Dyes. The *cis*-[Ru(LL)($dcbH_2$)$(NCS)_2$] dye sensitizers were prepared based on the one-pot procedure.[11,12] Briefly, the ruthenium *p*-cymene dimer, [Ru(*p*-cymene)Cl_2]$_2$, was dissolved in DMF, and 2 equiv of ancillary LL ligand was added. The mixture was kept at 80 °C for 2 h under argon atmosphere. After this period, 2 equiv of $dcbH_2$ was added to the mixture, and the temperature was increased to 160 °C and kept at these conditions for 4 h. After that, a 10-fold excess of NaNCS was added to the mixture, and the temperature was decreased to 140 °C, keeping the reaction under these conditions for 4 h. Most of the solvent was distilled off under reduced pressure, and cold deionized water was added to yield a precipitate that was filtered and washed with water. The crude product was dissolved in a methanolic TBAOH solution, centrifuged to remove any residual particles, and loaded on a liquid column chromatography containing Sephadex LH-20 as the stationary phase and methanol as the eluent. The purification process was repeated three times. For Ru(pyr), an additional liquid column chromatography step was performed, employing silica as the stationary phase and methanol:acetonitrile 1:1 as the eluent. The pure fractions were concentrated, precipitated by adding HNO_3, filtered, washed with cold deionized water and ethyl ether, and dried in a vacuum oven. The compounds were isolated as their monodeprotonated tetrabutylammonium (TBA) salts.

Ru(phen) (Yield = 35%. Anal. Calcd for (TBA)$C_{26}H_{15}N_6O_4RuS_2\cdot 3H_2O$: C, 53.83; H, 6.13; N, 10.46%; Found: C: 54.26; H, 6.07; N, 10.24%. NMR ^{1}H (DMF-d_7 + HNO_3, 500 MHz, δ/ppm): 9.78 (d, 1H, J = 5.8 Hz); 9.74 (d, 1H, J = 5.1 Hz); 9.25 (s, 1H); 9.06 (s, 1H); 8.97 (d, 1H, J = 8.3 Hz); 8.61 (d, 1H, J = 8.2 Hz); 8.45 (dd, 1H, J = 5.8 and 1.7 Hz); 8.43 (d, 1H, J = 8.9 Hz); 8.39 (dd, 1H, J = 8.3 and 5.2 Hz); 8.31 (d, 1H, J = 8.9 Hz); 8.20 (d, 1H, J = 5.3 Hz); 7.98 (d, 1H, J = 5.9 Hz); 7.68 (dd, 1H, J = 8.1 and 5.3 Hz); 7,59 (dd, 2H, J = 5.9 and 1.8 Hz)).

DOI: 10.1021/acsami.9b15448
ACS Appl. Mater. Interfaces 2019, 11, 43223−43234

Ru(pyr) (Yield = 35%. Anal. Calcd for (TBA)$C_{34}H_{21}N_8O_4RuS_2 \cdot 4H_2O$: C, 55.33; H, 6.04; N, 11.62%; Found: C: 55.33; H, 6.02; N, 11.55%. NMR ^{1}H (DMF-d_7 + HNO_3, 500 MHz, δ/ppm): 9.81 (d, 1H, J = 5.8 Hz); 9.80 (d, 1H, J = 5.5 Hz); 9.26 (s, 1H); 9.07 (s, 1H); 8.55 (d, 1H, J = 9.5 Hz); 8.47 (dd, 1H, J = 5.8 and 1.7 Hz); 8.43 (d, 1H, J = 3.9 Hz); 8.42 (s, 1H); 8.33 (d, 1H, J = 5.9 Hz); 8;10 (d, 1H, J = 5.9 Hz); 7.70 (d, 1H, J = 5.9 Hz); 7.68 (t, 2H, J = 2.1 Hz); 7.60 (dd, 1H, J = 6.0 e 1.7 Hz); 7.41 (t, 2H, J = 2.2 Hz); 6.67 (t, 2H, J = 2.1 Hz); 6.53 (t, 2H, J = 2.1 Hz)).

Ru(ind) (Yield = 43%. Anal. Calcd for (TBA)$C_{42}H_{25}N_8O_4RuS_2 \cdot 4H_2O$: C, 58.77; H, 5.87; N, 10.63%; Found: C: 58.40; H, 5.84; N, 10.59%. NMR ^{1}H (DMF-d_7 + HNO_3, 500 MHz, δ/ppm): 9.94 (d, 1H, J = 5.7 Hz); 9.87 (d, 1H, J = 5.7 Hz); 9.29 (s, 1H); 9.11 (s, 1H); 8.58 (d, 1H, J = 5.7 Hz); 8.50 (dd, 1H, J = 5.8 and 1.7 Hz); 8.44 (d, 1H, J = 5.8 Hz); 8.21 (d, 1H, J = 5.5 Hz); 8.15 (d, 1H, J = 9.4 Hz); 8.02 (d, 1H); 7.86 (dd, 1H, J = 7.1 and 1.3 Hz); 7.85 (d, 1H, J = 6.0 Hz); 7.76 (dd, 1H, J = 6.7 and 1.4 Hz); 7.75 (d, 1H, J = 7.7 Hz); 7.70 (d, 1H, J = 7.6 Hz); 7.62 (dd, 1H, J = 6.0 and 1.7 Hz); 7.27 (m, 6H); 7.08 (d, 1H, J = 3.3 Hz); 6.94 (d, 1H, J = 3.4 Hz)).

Ru(cbz) (Yield = 55%. Anal. Calcd for (TBA)$C_{50}H_{29}N_8O_4RuS_2 \cdot 4H_2O$: C, 61.66; H, 5.72; N, 9.81%; Found: C: 61.71; H, 5.83; N, 9.67%. NMR ^{1}H (DMF-d_7 + HNO_3, 500 MHz, δ/ppm): 10.09 (d, 1H, J = 5.6 Hz); 9.91 (d, 1H, J = 5.7 Hz); 9.32 (s, 1H); 9.15 (s, 1H); 8.75 (d, 1H, J = 5.6 Hz); 8.60 (d, 1H, J = 5.8 Hz); 8.52 (d, 1H, J = 5.8 Hz); 8.41 (d, 2H, J = 7.6 Hz); 8.31 (m, 4H); 8.01 (d, 1H, J = 5.8 Hz); 7.80 (d, 1H, J = 9.3 Hz); 7.69 (d, 1H, J = 9.1 Hz); 7.49 (m, 12H)).

Thin Film Preparation. Transparent mesoporous nanocrystalline TiO_2 thin films for electrochemical and spectroscopic measurements were prepared over transparent FTO conductive substrates as previously described in the literature.[13] Mesoporous thin films of tin(IV) indium-doped oxide nanoparticles (oxidized nanoITO) were prepared as previously described.[14] The as-prepared films were dyed by immersing them in 0.1 mmol L^{-1} sensitizer solutions in acetonitrile for at least 24 h to ensure saturation surface coverage. Prior to use, the films were soaked in neat acetonitrile for at least 1 h to remove any weakly adsorbed molecules from the surface to minimize dye desorption during the course of the experiments. Sensitized thin films were positioned at 45° angle in glass cuvettes filled with the desired acetonitrile solutions and purged with argon gas for a minimum of 30 min prior to electrochemical or spectroscopic studies.

Methods. Nuclear magnetic resonance spectra (NMR) were obtained using a Varian (500 MHz) spectrometer at 300 K. Residual solvent signals were used as the internal standard. The Fourier transform infrared (FTIR) spectra were recorded from 4000 to 500 cm^{-1} on a PerkinElmer Spectrum Two 160000A spectrometer using an attenuated total reflectance (ATR) accessory. Electronic absorption spectra were recorded using an Agilent 8453 diode-array spectrophotometer. Photoluminescence (PL) spectra were recorded in quartz cuvettes (1.000 cm path length) using a Cary Eclipse spectrofluorometer after the samples were purged with argon for 30 min.

Electrochemistry. Cyclic voltammetry and differential pulse voltammetry of the compounds dissolved in 0.1 mol L^{-1} $TBAPF_6$/acetonitrile solution were performed using a μAutolab III potentiostat/galvanostat (Autolab) using a standard three-electrode arrangement comprised of a glassy carbon working electrode (Metrohm), a Pt rod counter electrode (Metrohm), and a Ag wire as a pseudoreference electrode.

For the sensitized thin oxide films, data were obtained using a WaveNow potentiostat (Pine Research Instrumentation, Inc.) coupled to an AvaSpec UL2048 UV−visible spectrometer and an AvaLight deuterium/halogen light source (Avantes), all controlled by the AfterMath software (Pine Research Instrumentation, Inc.). The electrochemical setup consisted of a standard three-electrode cell with sensitized thin films as the working electrodes, a Pt mesh as the counter electrode, and nonaqueous Ag/AgCl as the pseudoreference electrode. Experiments were performed in a 0.1 mol L^{-1} $TBAPF_6$/acetonitrile electrolyte. For spectroelectrochemical measurements, nanoITO films were used as the working electrodes, and applied potentials were held for ∼30 s before the UV−vis absorption spectrum was recorded. Concentration curves of the redox species, Ru^{3+} and Ru^{2+}, were analyzed as a function of the applied potential, from which formal reduction potentials, $E°(Ru^{3+/2+})$, were obtained. For chronoabsorptometry experiments, TiO_2 films were employed as working electrodes. To measure the apparent diffusion coefficients D_{app}, a potential step 500 mV more positive than $E°(Ru^{3+/2+})$ was applied for several minutes, and full UV−visible spectra were taken at fixed time intervals.

The ferrocene/ferrocenium pair was used as the standard in all electrochemical experiments. All potentials were converted to the normal hydrogen electrode (NHE) through the use of the Fc^+/Fc half-wave potential, +630 mV vs NHE.[15]

Transient Absorption. The apparatus for nanosecond transient absorption has been previously described.[16] The laser fluence was adjusted to 1 mJ cm^{-2} for all experiments. Relative excited-state electron injection yields were measured by comparative actinometry[17] on the nanosecond time scale using a sensitized RuP|TiO_2, RuP = $[Ru(4,4'\text{-}(PO_3H_2)_2\text{-}2,2'\text{-bipyridine})(bpy)_2]^{2+}$, thin film immersed in pH 1 $HClO_4$ aqueous solution as the reference actinometer, Φ_{inj} = 1.[18]

DSSCs. *Preparation.* Mesoporous thin films of 0.196 cm^2 area and 11.6 ± 0.5 μm height were prepared by screen-printing the TiO_2 paste onto clean FTO glasses (8 Ω $\square^{-1}$), followed by equilibration under an ethanol saturated atmosphere for 6 min. The thin films were then dried at 125 °C for 6 min. The deposition process was repeated three times. After TiO_2 depositions, the films were sintered for 5 min at 325 °C, 5 min at 375 °C, 15 min at 450 °C, and 15 min at 500 °C.[19] Films thicknesses were measured by using a Tencor P-7 profiler. After sintering, the films were sensitized by immersing TiO_2 electrodes into 0.1 mmol L^{-1} ethanolic sensitizer solutions for 24 h. The Pt counter-electrodes were fabricated by the deposition of hexachloroplatinic acid on FTO and heating to 450 °C for 30 min. The two electrodes were sealed together with a Surlyn film heated to 110 °C in a custom-built sealing apparatus.[9] The mediator was placed between the electrodes through a hole drilled on the counter-electrode. The mediator was prepared by dissolving 38 mg of iodine, 59 mg of guanidinium thiocyanate, 0.38 mL of 4-*tert*-butylpyridine, and 0.80 mg of 1-butyl-3-methylimidazolium iodide in 85:15 v:v acetonitrile:valeronitrile to yield a 5 mL solution.

Characterization. For all DSSC measurements, at least four identical devices were prepared. Photocurrent action spectra and current−voltage curves were measured using a previously described Newport system.[3] The devices were illuminated through the photoanode side.

Optoelectronic transient and charge extraction measurements were tested on an in-lab built system, termed "STRiVE" (Sequential Time-Resolved current(i)-Voltage Experiments) with illumination through the counter-electrode side.[20,21] Cell current was measured by the voltage drop across a 1 Ohm resistor in series with the external circuit. This voltage was amplified by an instrument amplifier (INA 128, Texas Instruments). The amplified voltage as well as the operating voltage between the working and counter electrode could be simultaneously measured by a 16-bit data acquisition board (NI-6251) with a maximum sampling rate of 1.25 MHz. The cell was held at open or short circuit by fast solid-state switches (MOSFETs). Illumination was provided by an array of white LEDs (not a solar spectrum) and/or an array of colored LEDs controlled by fast solid-state switches with switching times of ∼250 ns. Potentials were applied to the cell using a PAR 362 scanning potentiostat. For transient photovoltage decay measurements, the cell voltage was set by the intensity of the white background LEDs, at open circuit. After a 45 s equilibration time, a pulse of blue LED light was superimposed on the background light. The voltage perturbation was recorded, and the decay could be easily fit to a single exponential decay. The magnitude of the perturbation was kept at ∼4 mV, controlled by the duration of the colored LED pulse, which was typically 10−500 μs. For charge extraction measurements, the cell was held at open circuit for 45 s under a given light intensity. The light was then turned off, and the cell was short circuited. The resulting current transient was recorded for 4 s and integrated to give the charge.

DOI: 10.1021/acsami.9b15448
ACS Appl. Mater. Interfaces 2019, 11, 43223−43234

RESULTS

Characterization of Ru(II) Dye Sensitizers. The UV–vis absorption spectra of all *cis*-[Ru(LL)(dcbH$_2$)(NCS)$_2$] sensitizers in DMF, Figure 2, exhibited two broad and intense

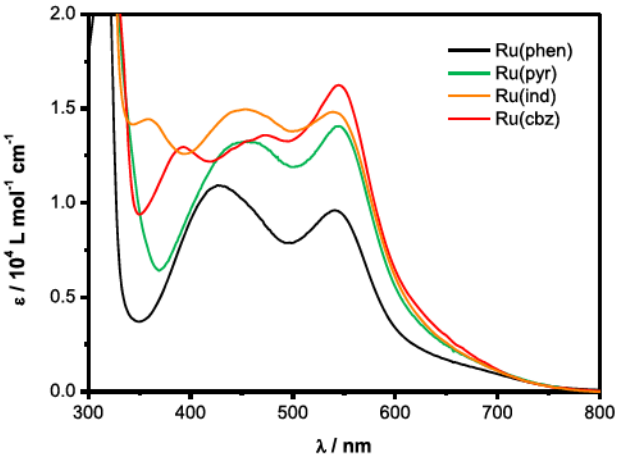

Figure 2. Absorption spectra of the *cis*-[Ru(LL)(dcbH$_2$)(NCS)$_2$] sensitizers in DMF, pH$_{app}$ 1.5.

absorption bands between 400 and 700 nm attributed to $d\pi(t_{2g})_{Ru} \rightarrow \pi^*_{polypyridyl\ ligands}$ metal-to-ligand charge transfer (MLCT) transitions.[22,23] The molar extinction coefficients of these bands were higher for the compounds containing N-heterocyclic substituents at the 4,7-positions of the phenanthroline ring in comparison to Ru(phen), Table 1, as described in literature for similar compounds having π-conjugated substituents.[9,24−26] In the UV region, the spectra also exhibited absorption bands ascribed to $\pi \rightarrow \pi^*$ and $n \rightarrow \pi^*$ intraligand transitions from the LL and dcbH$_2$ polypyridyl ligands.[26] Upon excitation of the low-energy MLCT absorption bands, the compounds displayed weak photoluminescence in acetonitrile with maxima around 805 nm. The PL spectra were broad and nonstructured, as typically observed in the emission from the lowest lying ^{3}MLCT excited state for similar ruthenium *tris*-heteroleptic compounds.[27−29]

Spectroelectrochemical experiments using nanoITO thin films sensitized by *cis*-[Ru(LL)(dcbH$_2$)(NCS)$_2$] immersed in 0.1 mol L^{-1} TBAPF$_6$/CH$_3$CN electrolyte, in which absorbance changes were monitored after the application of an increasingly positive electrochemical potential, provided information on $Ru^{3+/2+}$ mol fraction as a function of the applied potential. Electrochemical oxidation of the dyes resulted in a bleach of the MLCT bands and growth of weak, broad absorption bands at longer wavelengths (>600 nm), indicative of the one-electron oxidation of the compounds from Ru^{2+} to Ru^{3+}. The potential where equal concentrations of Ru^{2+} and Ru^{3+} were observed was taken as the formal reduction potential, $E°(Ru^{3+/2+})$.[5] The $E°(Ru^{3+/2+})$ values determined this way were 1.05 ± 0.02 V vs. NHE for all compounds and were the same, within the experimental error, in comparison to the values measured by cyclic and differential pulse voltammetry for the complexes dissolved in acetonitrile electrolyte solution.

The excited-state reduction potentials $E°(Ru^{3+/2+*})$ of the sensitizers were estimated through a free-energy cycle, $E°(Ru^{3+/2+*}) = E°(Ru^{3+/2+}) - \Delta G_{ES}$, in which ΔG_{ES} is the Gibbs free energy stored in the ^{3}MLCT excited-state determined from the emission onsets, Table 1. ΔG_{ES} decreased with the increase on the size of the aromatic substituent and resulted in less negative $E°(Ru^{3+/2+*})$ potentials.

Kinetics: Chronoabsorptometry and Transient Absorption. Lateral self-exchange intermolecular $Ru^{3+/2+}$ electron transfer on nanocrystalline TiO$_2$ surfaces, referred to as "hole-hopping", was quantified by chronoabsorptometry.[5,30,31] In contrast to the spectroelectrochemical experiments, a single potential step 500 mV more positive than $E°(Ru^{3+/2+})$ was applied to the films, and the oxidation rates were quantified spectroscopically. Single-wavelength kinetics were monitored at the low-energy MLCT maxima (530 nm) and were plotted as the Ru^{2+} mole fraction, that corresponds to the normalized absorbance change, ΔA, versus the square root of time, $t^{1/2}$, Figure 3.

The first 60% of the oxidation[5,6,31,32] was fit to the Anson equation, eq 1, in which d is the film thickness, and provided the apparent diffusion coefficient D_{app}, Table 2. The D_{app} values followed the trend Ru(phen) > Ru(pyr) > Ru(ind) > Ru(cbz) and are on the order of 10^{-8} cm^2 s^{-1}, in agreement with the values published for other tris-heteroleptic *cis*-[Ru(NN)(dcbH$_2$)(NCS)$_2$]-type dyes.[3,33,34] The D_{app} values were also used to estimate the first-order effective rate constants for intermolecular hole-hopping, k_{hh}, by using the Dahms–Ruff equation,[5,30,35] eq 2, in which δ is the intermolecular distance between the molecules on the surface that was estimated based on the saturation surface coverage

Table 1. Selected Photophysical and Electrochemical Properties of the *cis*-[Ru(LL)(dcbH$_2$)(NCS)$_2$] Compounds

	absorption[a] λ_{max}/nm (ε/10^4 L mol^{-1} cm^{-1})				
compound	ligand-based	MLCT	ΔG_{ES}/eV[b]	$E°(Ru^{3+/2+})$[c,d,e]	$E°(Ru^{3+/2+*})$[d,e]
Ru(phen)	269 (4.4)	429 (1.1)	1.9	1.05	−0.85
	318 (2.4)	541 (0.94)			
Ru(pyr)	279 (4.2)	455 (1.3)	1.88	1.05	−0.83
	319 (4.0)	543 (1.4)			
Ru(ind)	270 (5.9)	451 (1.5)	1.87	1.05	−0.82
	318 (3.7)	541 (1.5)			
	359 (1.4)				
Ru(cbz)	277 (6.4)	473 (1.3)	1.81	1.05	−0.76
	319 (3.6)	545 (1.5)			
	392 (1.2)				

[a]Measured in DMF solution. [b]ΔG_{ES} is the Gibbs free energy stored in the ^{3}MLCT excited-state, estimated from the emission spectra in acetonitrile solutions. [c]Measured for sensitized nanoITO thin films. [d]$E°(Ru^{3+/2+})$ and $E°(Ru^{3+/2+*})$ are given in V versus NHE. [e]Standard deviations are ±0.02 V.

DOI: 10.1021/acsami.9b15448
ACS Appl. Mater. Interfaces 2019, 11, 43223−43234

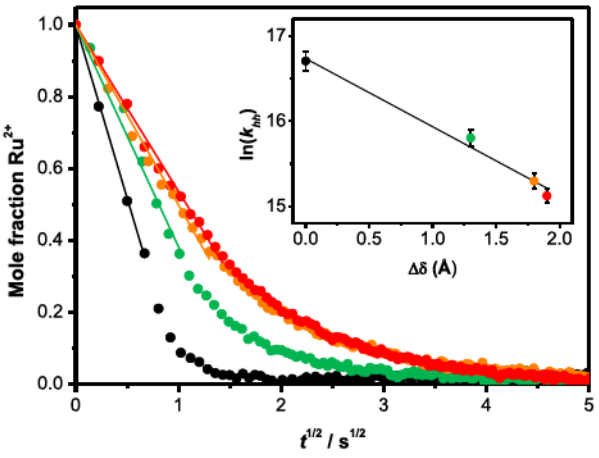

Figure 3. Changes in the mole fraction of the Ru^{2+} species as a function of the square root of time after the application of a potential step sufficient to oxidize the sensitizers Ru(phen) (black), Ru(pyr) (green), Ru(ind) (orange), or Ru(cbz) (red) anchored to TiO_2 thin films. The films were immersed in a 0.1 mol L^{-1} $TBAPF_6$/acetonitrile electrolyte. The absorption changes were monitored at 530 nm. Inset: $Ru^{3+/2+}$ lateral self-exchange rate constants, k_{hh}, versus the difference in intermolecular distance $\Delta\delta = \delta - \delta_{Ru(phen)}$. Error bars are given for the $\ln(k_{hh})$.

Γ_0,[5,6] accordingly to the method detailed in ref 5. The results are summarized in Table 2.

$$\Delta A = \frac{2D_{app}^{1/2}t^{1/2}}{d\pi^{1/2}} \quad (1)$$

$$D_{app} = \frac{k_{HH}\delta^2}{6} \quad (2)$$

The k_{hh} values followed the same trend as D_{app}, Ru(phen) > Ru(pyr) > Ru(ind) > Ru(cbz), and are of the same order of magnitude that was determined for similar *cis*-[Ru(LL)-$(dcbH_2)(NCS)_2$]-type dyes.[3] The increase in the steric bulk of the 4,7-substituents resulted in a decrease in the surface coverage caused by longer intermolecular distances that was tracked by the slower lateral $Ru^{3+/2+}$ self-exchange electron transfer. A similar trend was reported for bipyridine-based Ru(II) polypyridyl compounds[5,6,33]

Excitation of sensitized mesoporous TiO_2 films by pulsed 532 nm laser resulted in a bleach of the MLCT ground-state absorption bands and growth of a long-wavelength absorption. This observation is characteristic of the oxidized form of the dyes and have been previously assigned to $NCS^- \rightarrow Ru(III)$ ligand-to-metal charge transfer (LMCT) transitions,[36,37] Figure 4. These absorption changes are consistent with the formation of an interfacial charge-separation state characterized by surface-bound oxidized sensitizers and photoinjected electrons in the acceptor states of the mesoporous thin film.[3]

Relative injection quantum yields (Φ_{inj}) were quantified by comparative actinometry 20 ns after 532 nm pulsed light excitation and probed at the low-energy MLCT bleach maxima, with eq 3, where $\Delta A(\lambda_p)$ is the absorption change at the probe wavelength λ_p, $\Delta\varepsilon$ is the molar extinction coefficient difference between the ground and oxidized states, determined by spectroelectrochemical experiments, and $1-10^{-A}(\lambda_{exc})$ is the absorptance calculated from the absorbance at the excitation wavelength $A(\lambda_{ex})$.[17,38−41] A sensitized RuP|TiO_2, where RuP = $[Ru(4,4'\text{-}(PO_3H_2)_2\text{-}2,2'\text{-bipyridine})(bpy)_2]^{2+}$, thin film immersed in pH 1 $HClO_4$ aqueous solution ($\Delta\varepsilon$ (450 nm) = −10 000 L mol^{-1} cm^{-1}) was employed as an actinometric standard as previously described with $\Phi_{inj} = 1$.[18] The ΔA magnitude was taken 20 ns after the laser pulse to ensure signal was acquired beyond the rise time of the instrument, and only 7−11% of the initial amplitude was lost. The calculated Φ_{inj} values are summarized in Table 3 and were sensitive to the identity of the aromatic substituents.

$$\Phi_{inj}^{sample} = \left(\frac{\Delta A_{sample}(\lambda_p)}{\Delta A_{ref}(\lambda_p)} \times \frac{\Delta\varepsilon_{ref}(\lambda_p)}{\Delta\varepsilon_{sample}(\lambda_p)} \times \frac{1-10^{-A_{ref}(\lambda_{exc})}}{1-10^{-A_{sample}(\lambda_{exc})}}\right) \times \Phi_{inj}^{ref} \quad (3)$$

Back-electron transfer kinetics of the injected electron with the oxidized dye were monitored at 470 nm after pulsed 532 nm excitation of sensitized TiO_2 mesoporous films immersed in neat acetonitrile at open-circuit conditions, Figure 5. The transient data were nonexponential but were well-modeled by the Kohlraush−William−Watts (KWW) stretched exponential function,[42,43] eq 4, where A_0 is the initial transient absorption amplitude, k is the characteristic observed rate constant, and β is inversely proportional to the width of an underlying Lévy distribution of the rate constants, $0 < \beta < 1$.

Representative average back-electron transfer rate constants, k_{bet}, calculated as the first moment in the distribution,[44] were obtained from eq 5, where Γ is the gamma function and β = 0.2 for all measurements, and are summarized in Table 3. The back-electron transfer reaction was significantly faster for unsubstituted Ru(phen) and slower for Ru(cbz).

$$A(t) = A_0\exp(-kt)^{\beta} \quad (4)$$

$$k_{bet} = \left[\frac{1}{k\beta}\Gamma\left(\frac{1}{\beta}\right)\right]^{-1} \quad (5)$$

Regeneration of the oxidized dye by iodide ($E°(I_2^{\bullet-}/2I^-)$ = 0.93 V vs NHE)[45] was investigated by the recovery kinetics of

Table 2. Relevant Surface and Electrochemical Properties of the *cis*-$[Ru(LL)(dcbH_2)(NCS)_2]$ Compounds Anchored to TiO_2 Films[a]

compound	$D_{app}/10^{-8}$ cm^2 s^{-1}	$\Gamma_0/10^{-8}$ mol cm^{-2} μm^{-1}	δ/nm	$k_{hh}/10^6$ s^{-1}	H_{DA}/meV
Ru(phen)	5.1 ± 0.5	3.1 ± 0.3	1.48 ± 0.05	14 ± 2	3.8
Ru(pyr)	2.5 ± 0.2	2.4 ± 0.2	1.61 ± 0.06	5.7 ± 0.7	2.4
Ru(ind)	2.1 ± 0.2	2.2 ± 0.2	1.66 ± 0.06	4.4 ± 0.4	2.1
Ru(cbz)	1.7 ± 0.1	2.1 ± 0.2	1.67 ± 0.05	3.7 ± 0.3	1.9

[a] D_{app} = apparent diffusion coefficient; Γ_0 = saturation surface coverage; δ = intermolecular distance between the molecules on the surface; k_{hh} = first-order effective rate constants for intermolecular hole-hopping; H_{DA} = intermolecular electronic coupling matrix element.

DOI: 10.1021/acsami.9b15448
ACS Appl. Mater. Interfaces 2019, 11, 43223−43234

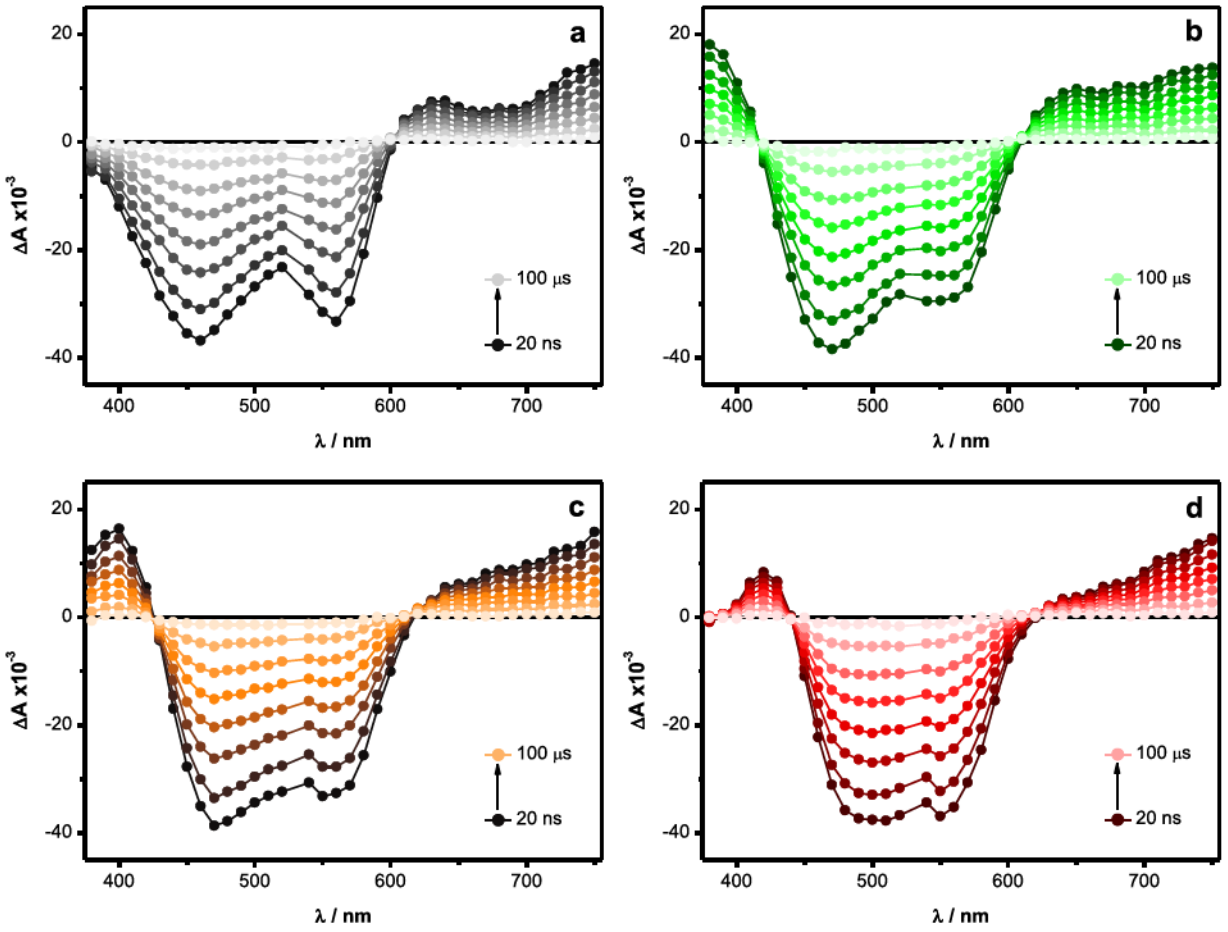

Figure 4. Transient absorption difference spectra after pulsed 532 nm excitation of TiO_2 thin films sensitized by (a) Ru(phen), (b) Ru(pyr), (c) Ru(ind), and (d) Ru(cbz), immersed in neat acetonitrile at open-circuit conditions.

Table 3. Rate Constants and Efficiencies of Some Electron Transfer Processes for Sensitized TiO_2 Films[a]

compound	Φ_{inj}	$k_{bet}/10^5$ s^{-1}	k_{cr}/s^{-1}	$k_{reg}/10^8$ L mol^{-1} s^{-1}
Ru(phen)	0.84 ± 0.03	1.2 ± 0.3	5 ± 1	4.01 ± 0.04
Ru(pyr)	0.79 ± 0.02	0.7 ± 0.1	13 ± 2	1.04 ± 0.02
Ru(ind)	0.58 ± 0.04	0.31 ± 0.07	9 ± 1	0.56 ± 0.02
Ru(cbz)	0.54 ± 0.01	0.18 ± 0.03	2.3 ± 0.9	0.34 ± 0.01

[a] Φ_{inj} = relative injection quantum yields; k_{bet} = average back-electron transfer rate constants; k_{cr} = average $TiO_2(e^-) \rightarrow I_3^-$ charge recombination rate constants; k_{reg} = second-order rate constants for dye regeneration.

the oxidized compound after pulsed 532 nm excitation of the dye-sensitized TiO_2 films immersed in 0.1 mol L^{-1} $TBAPF_6$/acetonitrile electrolyte at different TBAI concentrations. The kinetic data were fitted by the KWW function with $\beta = 0.2$. The observed rate constants, k_{obs}, exhibited a linear dependence on the I^- concentration, Figure 6. The second-order rate constants for dye-regeneration, k_{reg}, were taken as the slopes and followed the trend Ru(cbz) < Ru(ind) < Ru(pyr) < Ru(phen).

Recombination of injected electrons with I_3^- was monitored at 375 nm[3,46] after 532 nm excitation of dye-sensitized TiO_2 films immersed in 0.3 mol L^{-1} TBAI/acetonitrile solution and was found to be well-modeled by the KWW function with $\beta = 0.45$. Charge recombination rate constants k_{cr} followed the trend Ru(cbz) < Ru(phen) < Ru(ind) < Ru(pyr) and are in Table 3.

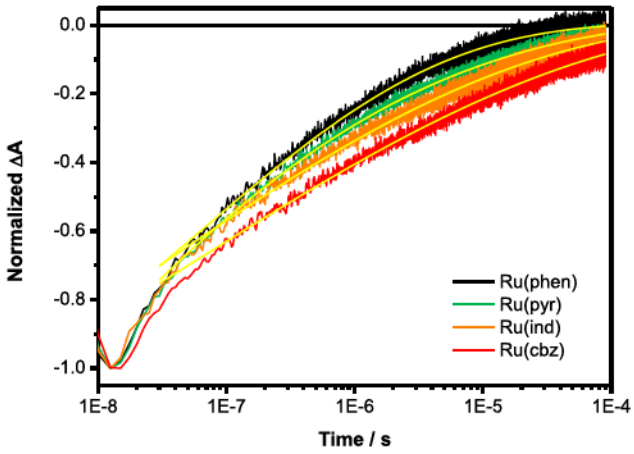

Figure 5. Absorption changes after pulsed 532 nm excitation of the sensitized TiO_2 films immersed in neat acetonitrile (λ = 470 nm). Overlaid traces in yellow are the best fits to the KWW kinetic model, $\beta = 0.2$.

Photoelectrochemical Performance and Optoelectronic Measurements. The photoelectrochemical performance of full-operating DSSCs was investigated to establish correlations between molecular structure, kinetics of electron transfer processes, and efficiency of the devices. Current–

DOI: 10.1021/acsami.9b15448
ACS Appl. Mater. Interfaces 2019, 11, 43223–43234

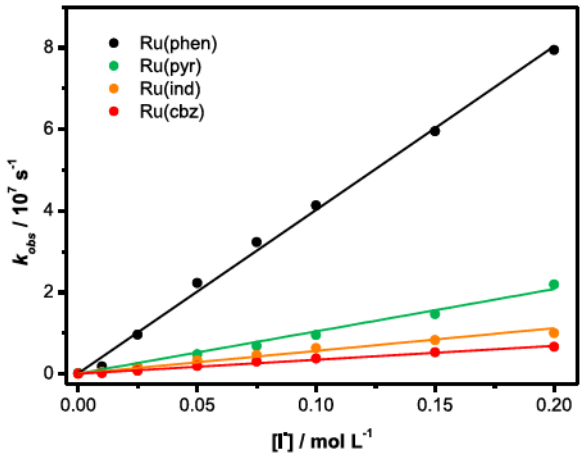

Figure 6. Observed rate constants (k_{obs}) as a function of the concentration of I^- after pulsed 532 nm excitation of dye-sensitized TiO_2 films immersed in 0.1 mol L^{-1} $TBAPF_6$/acetonitrile electrolyte.

voltage curves are shown in Figure 7-a, and the extracted photoelectrochemical parameters are in Table 4. Short-circuit current densities (J_{SC}), open-circuit voltages (V_{OC}), and overall conversion efficiencies (η) followed consistently the trend Ru(cbz) > Ru(phen) > Ru(ind) > Ru(pyr). Photocurrent action spectra determined for the solar cells, Figure 7-b, resembled the absorption spectra of the photoanodes. The maximum IPCE values followed the same trend observed for the other photoelectrochemical parameters.

Electron lifetimes as a function of total charge within the TiO_2 films were investigated by transient photovoltage decay (TVD) experiments using a custom-built instrument termed STRiVE.[20,21] The experiments were carried out at open-circuit conditions and in the small perturbation regime,[47] in which the kinetic responses of the DSSCs were monitored as they returned to steady state conditions following an external perturbation. The devices were illuminated through the counter electrode, so the highest electron concentration was generated at the TiO_2lelectrolyte interface.

Because the electron lifetime is a function of the incident light intensity, the measurements were repeated under a wide range of light intensities, Figure 8, and the measured lifetimes were evaluated as a function of the charge extracted from the device under matched conditions, Figure 9. The electron lifetimes were determined by fitting the photovoltage decay to a single exponential decay, eq 6, in which ΔV_0 is the initial amplitude and τ_n is the electron lifetime. The electron lifetimes at any electron concentration exhibited a clear dye-dependence that followed the trend Ru(pyr) < Ru(ind) < Ru(phen) < Ru(cbz) and displayed essentially the same sensitivity to the TiO_2 electron concentration.

$$V(t) = \Delta V_0 e^{-t/\tau_n} \quad (6)$$

DISCUSSION

The main goal of this study is to understand how aromatic substituents present in the 4 and 7 positions of the phenanthroline moiety can influence the electron transfer reactions that promote and inhibit light-to-electrical energy conversion with highly optimized sensitizers of the type *cis*-[Ru(LL)(dcbH$_2$)(NCS)$_2$]. Remarkably, these substituents had a significant influence on all the interfacial electron transfer processes even though the ground-state $Ru^{3+/2+}$ reduction potentials were held at parity. Photoelectrochemical characterization of DSSCs revealed that the small, systematic changes resulted in significant changes in the global power conversion efficiencies.

From a practical point of view, the Ru(cbz) dye was the most efficient, exhibiting the highest V_{OC} and J_{SC} in the series. To understand this behavior, below we discuss comprehensively the kinetics and efficiency of excited state electron injection (1), lateral hole-hopping (2), back-electron transfer to the oxidized sensitizer (3), regeneration through iodide oxidation (4), and recombination to the acceptors present in the electrolyte, I_{ox} = I_3^- or I_2, (5) shown in Figure 10 with correlation to the structure of the dyes.

Excited State Electron Injection (1). Excited state electron injection was rapid under all conditions investigated and could not be time-resolved with the apparatus that was utilized, $k_{inj} > 10^8$ s^{-1}. The relative quantum yields for excited state injection, Φ_{inj}, were quantified 20 ns after pulsed light excitation in neat CH_3CN. The values range from 0.54 to 0.84 and were correlated with the excited state reduction potentials. The most potent photoreductant Ru(phen)* had the highest yield, and Ru(cbz)* as the weakest displayed the lowest yield.

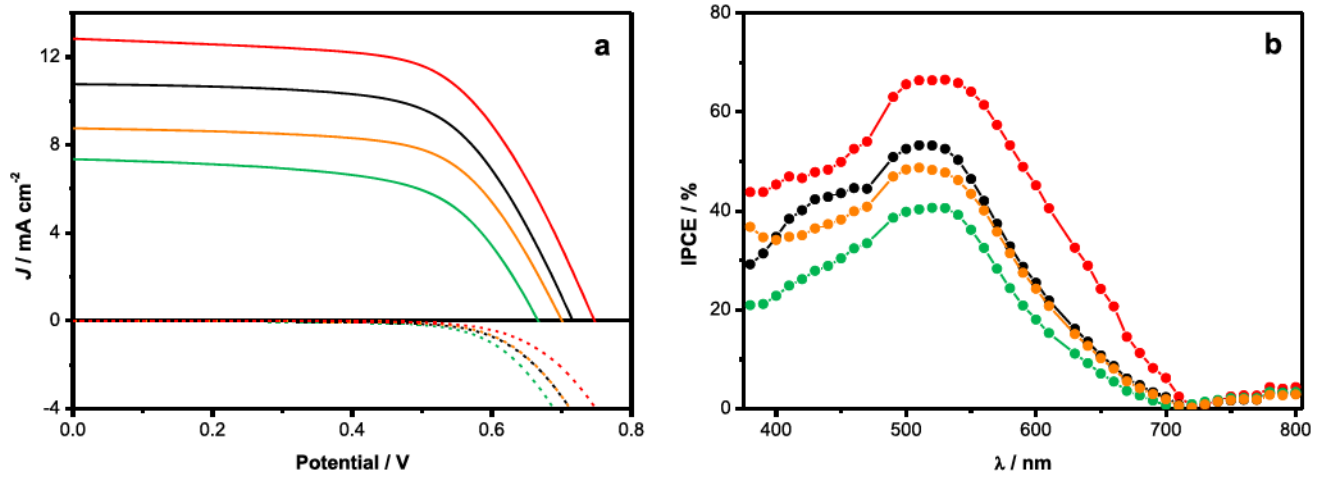

Figure 7. a) Current−voltage curves under 1 Sun (A.M. 1.5G) illumination (−) or in the dark (---) and (b) photocurrent action spectra measured for DSSCs sensitized by Ru(phen) (black), Ru(pyr) (green), Ru(ind) (orange), and Ru(cbz) (red).

DOI: 10.1021/acsami.9b15448
ACS Appl. Mater. Interfaces 2019, 11, 43223−43234

Table 4. Photoelectrochemical Parameters Determined for DSSCs Sensitized by *cis*-$[Ru(LL)(dcbH_2)(NCS)_2]$[a]

compound	J_{SC}/mA cm^{-2}	V_{OC}/V	ff	η/%	IPCE/% (λ_{max}/nm)
Ru(phen)	10.8 ± 0.9	0.74 ± 0.02	0.65 ± 0.03	5.4 ± 0.4	54 (510)
Ru(pyr)	7.4 ± 0.6	0.70 ± 0.02	0.65 ± 0.01	3.5 ± 0.3	41 (520)
Ru(ind)	8.7 ± 0.8	0.71 ± 0.02	0.67 ± 0.03	4.2 ± 0.4	49 (510)
Ru(cbz)	12.4 ± 0.4	0.76 ± 0.02	0.64 ± 0.01	6.1 ± 0.2	68 (520)

[a]J_{SC}= short-circuit current density; V_{OC} = open-circuit voltage; ff = fill factor; η = global conversion efficiency; IPCE = incident photon-to-current efficiency.

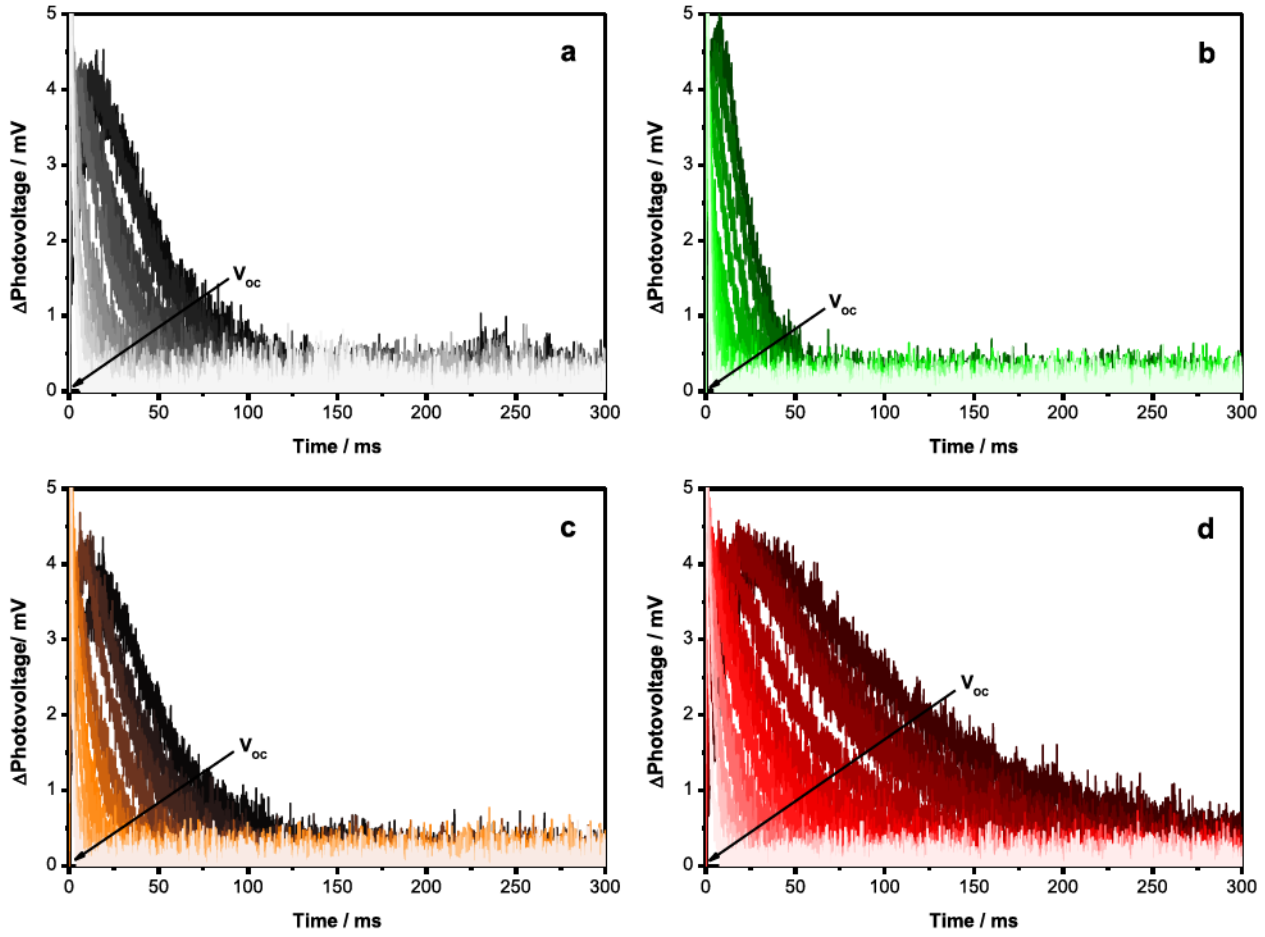

Figure 8. Transient photovoltage decay measurements for DSSCs sensitized by (a) Ru(phen), (b) Ru(pyr), (c) Ru(ind), and (d) Ru(cbz). The arrows indicate a V_{OC} increase approximately from 500 to 750 mV.

The presence of iodide in the ionic liquid electrolyte used for solar-to-electrical power generation precluded quantification of Φ_{inj}, yet it is likely that the injection yields were higher under the conditions used for the operational solar cell. High injection quantum yields are necessary for quantitative photocurrent yields and for high photovoltages in DSSCs.[3,48,49]

Hole-Hopping and Back-Electron Transfer (2 and 3). After dye-sensitized electron injection into the TiO_2 acceptor states, the surface-immobilized oxidized Ru^{3+} species can be translated away from the injection site by lateral self-exchange electron transfer without a loss of free energy. Marcus theory for nonadiabatic electron transfer was used to model the $Ru^{3+/2+}$ self-exchange on the surface of TiO_2, eq 7, where H_{DA} is the intermolecular electronic coupling matrix element between electron donor Ru^{2+} and electron acceptor Ru^{3+}, k_B is the Boltzmann constant, $\hbar$ is the reduced Planck constant, T is the absolute temperature, and λ is the total reorganization energy.[5,6,50]

$$k_{hh} = \left(\frac{2\pi}{\hbar}\right)\left(\frac{|H_{DA}|^2}{\sqrt{4\pi\lambda k_B T}}\right)e^{(-\lambda/4k_B T)} \quad (7)$$

At constant λ and T, k_{hh} depends only on the coupling matrix H_{DA}, which often decreases exponentially with intermolecular distance, eq 8, in which δ is the intermolecular distance between the donor and acceptor, β is an attenuation factor, and H^0_{DA} is the electronic coupling at van der Waals separation, δ_0.[51−54] The k_{hh} values, determined experimentally after a potential step was applied to TiO_2 electrodes with known sensitizer surface coverages, were used to quantify β values, eq 8, where $\Delta\delta$ is the difference between the calculated δ and the smallest δ in the series and k^0_{hh} is the hole-hopping rate constant for the reference compound Ru(phen).[6]

$$H_{DA} = H^0_{DA} e^{-(\beta/2)(\delta-\delta_0)} \quad (8)$$

DOI: 10.1021/acsami.9b15448
ACS Appl. Mater. Interfaces 2019, 11, 43223−43234

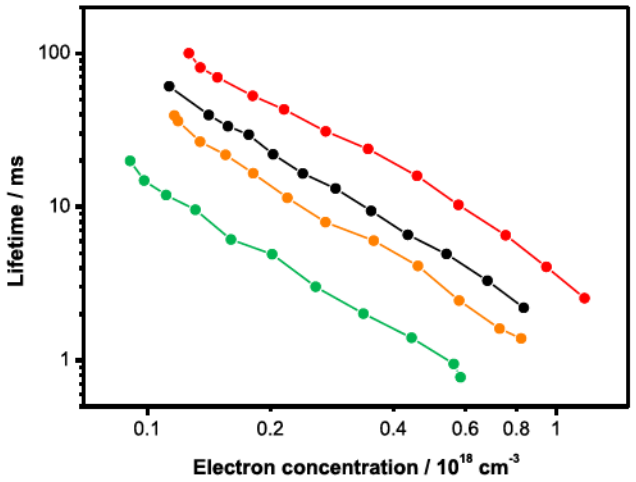

Figure 9. Electron lifetimes measured from the single-exponential decay in transient photovoltage measurements of DSSCs sensitized by Ru(phen) (black), Ru(pyr) (green), Ru(ind) (orange), or Ru(cbz) (red).

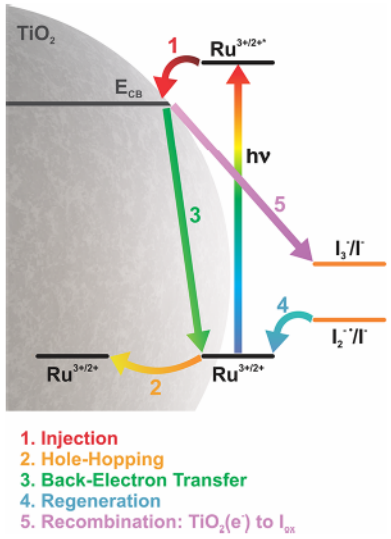

Figure 10. Schematic representation of electron transfer processes occurring after dye excitation.

$$k_{hh} = k_{hh}^{0} e^{-\beta\Delta\delta} \quad (9)$$

The experimental k_{hh} values displayed a good correlation with the intermolecular distances estimated from the measured saturation surface coverages. The exponential distance dependence suggests that the variation in k_{hh} for the different *cis*-[Ru(LL)(dcbH$_2$)(NCS)$_2$] complexes resulted mostly from a distance effect induced by the different steric bulk of the aromatic groups.[5,6] The attenuation factor was found to be β = 0.82 ± 0.07 Å^{-1}. Values previously reported for $Ru^{3+/2+}$ self-exchange for polypyridyl complexes anchored to a TiO_2 surface were β = 1.2 ± 0.2 Å^{-1}.[6]

The electronic coupling H_{DA} was estimated from the measured k_{hh} rate constants and eq 7 with the assumption that λ = 1 eV.[5,55] The H_{DA} values so obtained were found to increase from 1.9 to 3.8 meV in going from Ru(cbz) to Ru(phen), reflecting the effect of the intermolecular distance, Table 2. These values were significantly higher than those reported for [Ru(bpy′)$_2$(dcbH$_2$)]-type dyes, where bpy′ is a 4,4′-dialkyl substituted bpy ligand, anchored to nanocrystalline TiO_2, that ranged between 0.02 and 0.10 meV.[5] The stronger coupling likely arises from the isothiocyanate groups in *cis*-[Ru(LL)(dcbH$_2$)(NCS)$_2$] dyes whose geometric orientation enhances frontier orbital overlap of neighboring ruthenium complexes.[33] For *cis*-[Ru(4,4′-(CH$_3$)$_2$-2,2′-bipyridine)-(dcbH$_2$)(NCS)$_2$], a H_{DA} = 130 meV value, estimated by *ab initio* Hartree–Fock calculations, was reported for intermolecular hole exchange over a TiO_2 surface.[33]

Recent reports revealed that the hole-hopping rates are correlated to the back-electron transfer rate constants.[3,7,8] Rapid hole-hopping promotes the formation of an encounter complex between the injected electron and the oxidized dye sensitizer $TiO_2(e^-)$ + S→ $TiO_2(e^-)$I-S$^+$ prior to charge recombination.[7,8] Indeed, the sensitizer trend in k_{hh} and k_{bet} values were the same, Ru(phen) > Ru(pyr) > Ru(ind) > Ru(cbz). The results demonstrate that it is possible to control back-electron transfer through control of the $Ru^{3+/2+}$ self-exchange kinetics. Using the Ru(cbz) sensitizer with the slowest hole-hopping resulted in the most sluggish kinetics for the unwanted back-electron transfer reaction.

Regeneration through Iodide (4). It has previously been shown that the sensitizer ground-state reduction potential is a good indicator of the regeneration rate constant, k_{reg}.[3,56,57] All four sensitizers investigated in this work exhibited the same $E°(Ru^{3+/2+})$ and hence the same thermodynamic driving force for regeneration by iodide.[45] Regeneration was first-order in the iodide concentration. Surprisingly, a 12-fold increase in k_{reg} for Ru(phen) was observed in comparison to Ru(cbz). The other sensitizers showed intermediate values with a trend that followed the number of aromatic rings on the phenanthroline ligand. Therefore, the steric hindrance imparted by these aromatic rings is envisioned to have a deleterious role in sensitizer regeneration. Density functional theory (DFT) calculations demonstrated that Ru(cbz) has a molecular volume about two times larger than that of Ru(phen) that may restrict access of iodide to the metal center in accordance with the experimental results presented herein.[58] Furthermore, it has been demonstrated that fast intermolecular hole-hopping results in higher regeneration yields in solid-state DSSCs.[59,60] A correlation between k_{hh} and k_{reg} also exists for this series of dyes, suggesting that hole hopping may also facilitate dye regeneration in liquid electrolyte based DSSCs.

It is important to note that for all four sensitizers k_{reg} was much larger than k_{bet}. In the operational solar cells, in which high iodide concentrations are present, regeneration yields Φ_{reg} of unity are expected at short-circuit conditions. At the maximum power-point, charge recombination is faster, and back-electron transfer may become a competitive pathway.[3]

Recombination to I_{ox} (5). Recombination of the injected electrons with the oxidized form of the redox mediator, I_{ox}, was also sensitive to the sensitizer molecular structure. The k_{cr} values measured after pulsed light excitation where I_3^- was the predominant acceptor followed the trend Ru(pyr) > Ru(ind) > Ru(phen) > Ru(cbz). This trend indicates that increased sensitizer steric bulk inhibits the approach of I_3^- to the TiO_2 surface, suppressing charge recombination, in a similar fashion to what was observed for regeneration.[61] Despite Ru(phen) being the smallest dye in the series, the absence of substituents resulted in a more compact, densely packed dye layer on the TiO_2 surface,[58] highlighted by the significantly higher surface coverage and smaller intermolecular distance, Table 2, resulting in the second smallest k_{cr} value in the series.

DOI: 10.1021/acsami.9b15448
ACS Appl. Mater. Interfaces 2019, 11, 43223–43234

Additionally, the electron lifetimes, i.e., the average time an electron remains in the TiO_2 film before recombination processes, were investigated in operational DSSCs by transient photovoltage decay. The trend in electron lifetimes with each sensitizer at a fixed electron concentration were the same as those measured after pulsed light excitation. The sensitizer Ru(cbz) provided the longest lifetime of the injected electrons that emanates from this slow recombination with the oxidized redox mediator.

Energy Conversion Efficiencies and Electron Transfer. The short circuit photocurrent density, J_{SC}, is equal to the fraction of light that is absorbed, the quantum yield for excited state injection, and the fraction of injected electrons that reach the external circuit. The J_{SC} trend Ru(pyr) < Ru(ind) < Ru(phen) < Ru(cbz) tracked the relative contributions from the excited state injection yield and the charge recombination kinetics. Injection yields and electron lifetimes also directly influence the maximum voltage output of a DSSC. The diode model predicts a 59 mV decrease in V_{OC} for every order of magnitude increase in charge recombination.[48,56,62] Results extracted from the current−voltage curves reveal: V_{OC} Ru(pyr) < Ru(ind) < Ru(phen) < Ru(cbz). The most optimal photoelectrochemical performance of the Ru(cbz) sensitizer, that contains the bulkiest aromatic substituent, originates mainly from slow recombination that overcomes even the most sluggish regeneration and least efficient injection in the series.

■ CONCLUSIONS

A series of *cis*-[Ru(LL)($dcbH_2$)$(NCS)_2$] compounds was investigated as dye sensitizers for DSSCs. The use of different N-heterocyclic aromatic substituents at the 4,7-positions of the 1,10-phenanthroline moiety allowed modification of the molecular size of the sensitizers and the energy stored in the excited state, while maintaining the same ground-state $Ru^{3+/2+}$ reduction potentials. The injection quantum yields tracked the stabilization of the excited state by the presence of aromatic groups. Through increase of the intermolecular distance between the dye molecules on the TiO_2 surface, the lateral self-exchange and back-electron transfer reactions were retarded. Dye regeneration and recombination of the injected electrons to oxidized mediators were sensitive to the steric bulk and packing of the molecules on the oxide surface. The global efficiencies, V_{OC}, and J_{SC} of full operating solar cells followed consistently the trend Ru(pyr) < Ru(ind) < Ru(phen) < Ru(cbz). The most optimal performance of Ru(cbz) was ascribed to the significantly smaller recombination losses that overcome even the most sluggish regeneration and least efficient injection in the series. Transient photovoltage and transient absorption experiments both revealed significantly slower recombination to oxidized mediators as the size of the aromatic substituents increased. We believe that the results presented herein can help to guide the molecular engineering to the discovery of new and more efficient dyes, avoiding energy losses by competitive electron transfer processes.

■ AUTHOR INFORMATION

Corresponding Authors

*E-mail: andre.polo@ufabc.edu.br.
*E-mail: gjmeyer@email.unc.edu.

ORCID

Andressa V. Müller: 0000-0002-3999-7798
Kleber T. de Oliveira: 0000-0002-9131-4800
Gerald J. Meyer: 0000-0002-4227-6393
André S. Polo: 0000-0001-7298-1619

Notes

The authors declare no competing financial interest.

■ ACKNOWLEDGMENTS

A.V.M., A.S.P., and K.T.O. are grateful to Fundação de Amparo à Pesquisa do Estado de São Paulo (FAPESP) for financial support (Grants 2016/21993-6, 2018/00106-7, 2016/24020-9, and 2018/08038-0). A.V.M. and A.S.P thank the Multiuser Central Facilities (UFABC) for the experimental support. The authors thank the National Science Foundation (Grant 1800022) for support of this research.

■ REFERENCES

(1) Durrant, J. R.; Haque, S. A.; Palomares, E. Towards Optimisation of Electron Transfer Processes in Dye Sensitised Solar Cells. *Coord. Chem. Rev.* **2004**, *248* (13), 1247−1257.

(2) Pashaei, B.; Shahroosvand, H.; Graetzel, M.; Nazeeruddin, M. K. Influence of Ancillary Ligands in Dye-Sensitized Solar Cells. *Chem. Rev.* **2016**, *116* (16), 9485−9564.

(3) Sampaio, R. N.; Müller, A. V.; Polo, A. S.; Meyer, G. J. Correlation Between Charge Recombination and Lateral Hole-Hopping Kinetics in a Series of cis-Ru(phen′)(dcb)(NCS)2 Dye-Sensitized Solar Cells. *ACS Appl. Mater. Interfaces* **2017**, *9* (39), 33446−33454.

(4) Reynal, A.; Forneli, A.; Martinez-Ferrero, E.; Sánchez-Díaz, A.; Vidal-Ferran, A.; O'Regan, B. C.; Palomares, E. Interfacial Charge Recombination Between e^--TiO_2 and the I^-/I_3^-; Electrolyte in Ruthenium Heteroleptic Complexes: Dye Molecular Structure-Open Circuit Voltage Relationship. *J. Am. Chem. Soc.* **2008**, *130* (41), 13558−13567.

(5) DiMarco, B. N.; Motley, T. C.; Balok, R. S.; Li, G.; Siegler, M. A.; O'Donnell, R. M.; Hu, K.; Meyer, G. J. A Distance Dependence to Lateral Self-Exchange across Nanocrystalline TiO_2. A Comparative Study of Three Homologous RuIII/II Polypyridyl Compounds. *J. Phys. Chem. C* **2016**, *120* (26), 14226−14235.

(6) Motley, T. C.; Brady, M. D.; Meyer, G. J. Influence of 4 and 4′ Substituents on RuIII/II Bipyridyl Self-Exchange Electron Transfer Across Nanocrystalline TiO2 Surfaces. *J. Phys. Chem. C* **2018**, *122* (34), 19385−19394.

(7) Moia, D.; Szumska, A.; Vaissier, V.; Planells, M.; Robertson, N.; O'Regan, B. C.; Nelson, J.; Barnes, P. R. F. Interdye Hole Transport Accelerates Recombination in Dye Sensitized Mesoporous Films. *J. Am. Chem. Soc.* **2016**, *138* (40), 13197−13206.

(8) Sampaio, R. N.; DiMarco, B. N.; Meyer, G. J. Activation Energies for Electron Transfer from TiO2 to Oxidized Dyes: A Surface Coverage Dependence Correlated with Lateral Hole Hopping. *ACS Energy Lett.* **2017**, *2* (10), 2402−2407.

(9) Müller, A. V.; Ramos, L. D.; Frin, K. P. M.; de Oliveira, K. T.; Polo, A. S. A High Efficiency Ruthenium(II) tris-Heteroleptic Dye Containing 4,7-dicarbazole-1,10-phenanthroline for Nanocrystalline Solar Cells. *RSC Adv.* **2016**, *6* (52), 46487−46494.

(10) Ramos, L. D.; Sampaio, R. N.; de Assis, F. F.; de Oliveira, K. T.; Homem-De-Mello, P.; Patrocinio, A. O. T.; Frin, K. P. M. Contrasting Photophysical Properties of Rhenium(I) Tricarbonyl Complexes Having Carbazole Groups Attached to the Polypyridine Ligand. *Dalton Trans* **2016**, *45* (29), 11688−11698.

(11) Müller, A. V.; Polo, A. S. Mechanistic Insights into the Stepwise Assembly of Ruthenium(II) Tris-heteroleptic Compounds. *Inorg. Chem.* **2018**, *57* (21), 13829−13839.

(12) Wang, P.; Zakeeruddin, S. M.; Moser, J. E.; Nazeeruddin, M. K.; Sekiguchi, T.; Grätzel, M. A Stable Quasi-Solid-State Dye-Sensitized Solar Cell with an Amphiphilic Ruthenium Sensitizer and Polymer Gel Electrolyte. *Nat. Mater.* **2003**, *2* (6), 402−407.

DOI: 10.1021/acsami.9b15448
ACS Appl. Mater. Interfaces 2019, 11, 43223−43234

(13) Heimer, T. A.; D'Arcangelis, S. T.; Farzad, F.; Stipkala, J. M.; Meyer, G. J. An Acetylacetonate-Based Semiconductor-Sensitizer Linkage. *Inorg. Chem.* **1996**, *35* (18), 5319−5324.
(14) Farnum, B. H.; Morseth, Z. A.; Lapides, A. M.; Rieth, A. J.; Hoertz, P. G.; Brennaman, M. K.; Papanikolas, J. M.; Meyer, T. J. Photoinduced Interfacial Electron Transfer within a Mesoporous Transparent Conducting Oxide Film. *J. Am. Chem. Soc.* **2014**, *136* (6), 2208−2211.
(15) Pavlishchuk, V. V.; Addison, A. W. Conversion Constants for Redox Potentials Measured versus Different Reference Electrodes in Acetonitrile Solutions at 25°C. *Inorg. Chim. Acta* **2000**, *298* (1), 97−102.
(16) Argazzi, R.; Bignozzi, C. A.; Heimer, T. A.; Castellano, F. N.; Meyer, G. J. Enhanced Spectral Sensitivity from Ruthenium(II) Polypyridyl Based Photovoltaic Devices. *Inorg. Chem.* **1994**, *33* (25), 5741−5749.
(17) Bergeron, B. V.; Kelly, C. A.; Meyer, G. J. Thin Film Actinometers for Transient Absorption Spectroscopy: Applications to Dye-Sensitized Solar Cells. *Langmuir* **2003**, *19*, 8389−8394.
(18) Hu, K.; Sampaio, R. N.; Marquard, S. L.; Brennaman, M. K.; Tamaki, Y.; Meyer, T. J.; Meyer, G. J. A High-Valent Metal-Oxo Species Produced by Photoinduced One-Electron, Two-Proton Transfer Reactivity. *Inorg. Chem.* **2018**, *57* (1), 486−494.
(19) Ito, S.; Murakami, T. N.; Comte, P.; Liska, P.; Grätzel, C.; Nazeeruddin, M. K.; Grätzel, M. Fabrication of Thin Film Dye Sensitized Solar Cells with Solar to Electric Power Conversion Efficiency Over 10%. *Thin Solid Films* **2008**, *516* (14), 4613−4619.
(20) Barr, T. J.; Meyer, G. J. Evidence for First-Order Charge Recombination in Dye-Sensitized Solar Cells. *ACS Energy Lett.* **2017**, *2* (10), 2335−2340.
(21) Barr, T. J. *Interfacial Electron Transfer at Sensitized Nanocrystalline TiO2 Electrolyte Interfaces: Influence of Surface Electric Fields and Lewis-Acidic Cations*; The University of North Carolina at Chapel Hill, 2017.
(22) Juris, A.; Balzani, V.; Barigelletti, F.; Campagna, S.; Belser, P.; von Zelewsky, A. Ru(II) Polypyridine Complexes: Photophysics, Photochemistry, Eletrochemistry, and Chemiluminescence. *Coord. Chem. Rev.* **1988**, *84*, 85−277.
(23) Onozawa-Komatsuzaki, N.; Kitao, O.; Yanagida, M.; Himeda, Y.; Sugihara, H.; Kasuga, K. Molecular and Electronic Ground and Excited Structures of Heteroleptic Ruthenium Polypyridyl Dyes for Nanocrystalline TiO2 Solar Cells. *New J. Chem.* **2006**, *30* (5), 689−697.
(24) Wang, Z. S.; Koumura, N.; Cui, Y.; Takahashi, M.; Sekiguchi, H.; Mori, A.; Kubo, T.; Furube, A.; Hara, K. Hexylthiophene-Functionalized Carbazole Dyes for Efficient Molecular Photovoltaics: Tuning of Solar-Cell Performance by Structural Modification. *Chem. Mater.* **2008**, *20* (12), 3993−4003.
(25) Wu, S.-J.; Chen, C.-Y.; Li, J.-Y.; Chen, J.-G.; Lee, K.-M.; Ho, K.-C.; Wut, C.-G. Carbazole Containing Ru-based Photo-sensitizer for Dye-sensitized Solar Cell. *J. Chin. Chem. Soc.* **2010**, *57* (5B), 1127−1130.
(26) Sun, Y.; Onicha, A. C.; Myahkostupov, M.; Castellano, F. N. Viable Alternative to N719 for Dye-Sensitized Solar Cells. *ACS Appl. Mater. Interfaces* **2010**, *2* (7), 2039−2045.
(27) Carvalho, F.; Liandra-Salvador, E.; Bettanin, F.; Souza, J. S.; Homem-De-Mello, P.; Polo, A. S. Synthesis, Characterization and Photoelectrochemical Performance of a tris-heteroleptic Ruthenium-(II) Complex having 4,7-dimethyl-1,10-phenanthroline. *Inorg. Chim. Acta* **2014**, *414*, 145−152.
(28) Müller, A. V.; Mendonça, P. S.; Parant, S.; Duchanois, T.; Gros, P. C.; Beley, M.; Polo, A. S. Effects of Methyl-Substituted Phenanthrolines on the Performance of Ruthenium(II) Dye-Sensitizers. *J. Braz. Chem. Soc.* **2015**, *26*, 2224−2232.
(29) Nazeeruddin, M. K.; Zakeeruddin, S. M.; Humphry-Baker, R.; Jirousek, M.; Liska, P.; Vlachopoulos, N.; Shklover, V.; Fischer, C. H.; Grätzel, M. Acid-Base Equilibria of (2,2′-bipyridyl-4,4′-dicarboxylic acid)ruthenium(II) Complexes and the Effect of Protonation on Charge-Transfer Sensitization of Nanocrystalline Titania. *Inorg. Chem.* **1999**, *38* (26), 6298−6305.
(30) Hu, K.; Meyer, G. J. Lateral Intermolecular Self-Exchange Reactions for Hole and Energy Transport on Mesoporous Metal Oxide Thin Films. *Langmuir* **2015**, *31* (41), 11164−11178.
(31) Bonhôte, P.; Gogniat, E.; Tingry, S.; Barbé, C.; Vlachopoulos, N.; Lenzmann, F.; Comte, P.; Grätzel, M. Efficient Lateral Electron Transport inside a Monolayer of Aromatic Amines Anchored on Nanocrystalline Metal Oxide Films. *J. Phys. Chem. B* **1998**, *102* (9), 1498−1507.
(32) Trammell, S. A.; Meyer, T. J. Diffusional Mediation of Surface Electron Transfer on TiO2. *J. Phys. Chem. B* **1999**, *103* (1), 104−107.
(33) Wang, Q.; Zakeeruddin, S. M.; Nazeeruddin, M. K.; Humphry-Baker, R.; Grätzel, M. Molecular Wiring of Nanocrystals: NCS-Enhanced Cross-Surface Charge Transfer in Self-Assembled Ru-Complex Monolayer on Mesoscopic Oxide Films. *J. Am. Chem. Soc.* **2006**, *128* (13), 4446−4452.
(34) Ardo, S.; Meyer, G. J. Characterization of Photoinduced Self-Exchange Reactions at Molecule−Semiconductor Interfaces by Transient Polarization Spectroscopy: Lateral Intermolecular Energy and Hole Transfer across Sensitized TiO2 Thin Films. *J. Am. Chem. Soc.* **2011**, *133* (39), 15384−15396.
(35) Blauch, D. N.; Saveant, J. M. Dynamics of Electron Hopping in Assemblies of Redox Centers. Percolation and Diffusion. *J. Am. Chem. Soc.* **1992**, *114* (9), 3323−3332.
(36) Tachibana, Y.; Moser, J. E.; Grätzel, M.; Klug, D. R.; Durrant, J. R. Subpicosecond Interfacial Charge Separation in Dye-Sensitized Nanocrystalline Titanium Dioxide Films. *J. Phys. Chem.* **1996**, *100* (51), 20056−20062.
(37) Das, S.; Kamat, P. V. Spectral Characterization of the One-Electron Oxidation Product of cis-Bis(isothiocyanato)bis(4,4′-dicarboxylato-2,2′-bipyridyl) Ruthenium(II) Complex Using Pulse Radiolysis. *J. Phys. Chem. B* **1998**, *102* (45), 8954−8957.
(38) Gillaizeau-Gauthier, I.; Odobel, F.; Alebbi, M.; Argazzi, R.; Costa, E.; Bignozzi, C. A.; Qu, P.; Meyer, G. J. Phosphonate-Based Bipyridine Dyes for Stable Photovoltaic Devices. *Inorg. Chem.* **2001**, *40* (23), 6073−6079.
(39) Brady, M. D.; Troian-Gautier, L.; Sampaio, R. N.; Motley, T. C.; Meyer, G. J. Optimization of Photocatalyst Excited- and Ground-State Reduction Potentials for Dye-Sensitized HBr Splitting. *ACS Appl. Mater. Interfaces* **2018**, *10* (37), 31312−31323.
(40) Hanson, K.; Brennaman, M. K.; Ito, A.; Luo, H.; Song, W.; Parker, K. A.; Ghosh, R.; Norris, M. R.; Glasson, C. R. K.; Concepcion, J. J.; Lopez, R.; Meyer, T. J. Structure−Property Relationships in Phosphonate-Derivatized, RuII Polypyridyl Dyes on Metal Oxide Surfaces in an Aqueous Environment. *J. Phys. Chem. C* **2012**, *116* (28), 14837−14847.
(41) Hanson, K.; Losego, M. D.; Kalanyan, B.; Parsons, G. N.; Meyer, T. J. Stabilizing Small Molecules on Metal Oxide Surfaces Using Atomic Layer Deposition. *Nano Lett.* **2013**, *13* (10), 4802−4809.
(42) Williams, G.; Watts, D. C. Non-Symmetrical Dielectric Relaxation Behaviour Arising From a Simple Empirical Decay Function. *Trans. Faraday Soc.* **1970**, *66* (0), 80−85.
(43) Scher, H.; Montroll, E. W. Anomalous Transit-Time Dispersion in Amorphous Solids. *Phys. Rev. B* **1975**, *12* (6), 2455−2477.
(44) Lindsey, C. P.; Patterson, G. D. Detailed Comparison of the Williams−Watts and Cole−Davidson Functions. *J. Chem. Phys.* **1980**, *73* (7), 3348−3357.
(45) Boschloo, G.; Hagfeldt, A. Characteristics of the Iodide/Triiodide Redox Mediator in Dye-Sensitized Solar Cells. *Acc. Chem. Res.* **2009**, *42* (11), 1819−1826.
(46) Rowley, J. G.; Farnum, B. H.; Ardo, S.; Meyer, G. J. Iodide Chemistry in Dye-Sensitized Solar Cells: Making and Breaking I-I Bonds for Solar Energy Conversion. *J. Phys. Chem. Lett.* **2010**, *1* (20), 3132−3140.
(47) Barnes, P. R. F.; Miettunen, K.; Li, X.; Anderson, A. Y.; Bessho, T.; Gratzel, M.; O'Regan, B. C. Interpretation of Optoelectronic

DOI: 10.1021/acsami.9b15448
ACS Appl. Mater. Interfaces 2019, 11, 43223−43234

Transient and Charge Extraction Measurements in Dye-Sensitized Solar Cells. *Adv. Mater.* **2013**, *25* (13), 1881−1922.
(48) Kumar, A.; Santangelo, P. G.; Lewis, N. S. Electrolysis of Water at Strontium Titanate (SrTiO3) Photoelectrodes: Distinguishing between the Statistical and Stochastic Formalisms for Electron-Transfer Processes in Fuel-Forming Photoelectrochemical Systems. *J. Phys. Chem.* **1992**, *96* (2), 834−842.
(49) de Souza, J. d. S.; de Andrade, L. O. M.; Müller, A. V.; Polo, A. S. In *Nanoenergy: Nanotechnology Applied for Energy Production*; Souza, F. L., Leite, E. R., Eds.; Springer International Publishing: Cham, 2018; pp 69−106.
(50) Marcus, R. A.; Sutin, N. Electron Transfers in Chemistry and Biology. *Biochim. Biophys. Acta, Rev. Bioenerg.* **1985**, *811* (3), 265−322.
(51) Wenger, O. S.; Leigh, B. S.; Villahermosa, R. M.; Gray, H. B.; Winkler, J. R. Electron Tunneling Through Organic Molecules in Frozen Glasses. *Science* **2005**, *307* (5706), 99−102.
(52) Winkler, J. R.; Gray, H. B. Long-Range Electron Tunneling. *J. Am. Chem. Soc.* **2014**, *136* (8), 2930−2939.
(53) Edwards, P. P.; Gray, H. B.; Lodge, M. T. J.; Williams, R. J. P. Electron Transfer and Electronic Conduction through an Intervening Medium. *Angew. Chem., Int. Ed.* **2008**, *47* (36), 6758−6765.
(54) Closs, G. L.; Miller, J. R. Intramolecular Long-Distance Electron Transfer in Organic Molecules. *Science* **1988**, *240* (4851), 440−447.
(55) Moia, D.; Vaissier, V.; López-Duarte, I.; Torres, T.; Nazeeruddin, M. K.; O'Regan, B. C.; Nelson, J.; Barnes, P. R. F. The Reorganization Energy of Intermolecular Hole Hopping between Dyes Anchored to Surfaces. *Chem. Sci.* **2014**, *5* (1), 281−290.
(56) Robson, K. C. D.; Hu, K.; Meyer, G. J.; Berlinguette, C. P. Atomic Level Resolution of Dye Regeneration in the Dye-Sensitized Solar Cell. *J. Am. Chem. Soc.* **2013**, *135* (5), 1961−1971.
(57) Planells, M.; Pelleja, L.; Clifford, J. N.; Pastore, M.; De Angelis, F.; Lopez, N.; Marder, S. R.; Palomares, E. Energy Levels, Charge Injection, Charge Recombination and Dye Regeneration Dynamics for Donor-Acceptor π-Conjugated Organic Dyes in Mesoscopic TiO2 Sensitized Solar Cells. *Energy Environ. Sci.* **2011**, *4* (5), 1820−1829.
(58) Veiga, E. T.; Müller, A. V.; Ramos, L. D.; Frin, K. P. M.; Polo, A. S. Interrelationship between the Ancillary Ligand Structure, Acid−Base Properties, and TiO2 Surface Coverage of RuII Dyes. *Eur. J. Inorg. Chem.* **2018**, *2018* (23), 2680−2688.
(59) Moia, D.; Cappel, U. B.; Leijtens, T.; Li, X.; Telford, A. M.; Snaith, H. J.; O'Regan, B. C.; Nelson, J.; Barnes, P. R. F. The Role of Hole Transport between Dyes in Solid-State Dye-Sensitized Solar Cells. *J. Phys. Chem. C* **2015**, *119* (33), 18975−18985.
(60) Weisspfennig, C. T.; Hollman, D. J.; Menelaou, C.; Stranks, S. D.; Joyce, H. J.; Johnston, M. B.; Snaith, H. J.; Herz, L. M. Dependence of Dye Regeneration and Charge Collection on the Pore-Filling Fraction in Solid-State Dye-Sensitized Solar Cells. *Adv. Funct. Mater.* **2014**, *24* (5), 668−677.
(61) Murakami, T. N.; Koumura, N.; Yoshida, E.; Funaki, T.; Takano, S.; Kimura, M.; Mori, S. An Alkyloxyphenyl Group as a Sterically Hindered Substituent on a Triphenylamine Donor Dye for Effective Recombination Inhibition in Dye-Sensitized Solar Cells. *Langmuir* **2016**, *32* (4), 1178−1183.
(62) Li, F.; Jennings, J. R.; Wang, Q. Determination of Sensitizer Regeneration Efficiency in Dye-Sensitized Solar Cells. *ACS Nano* **2013**, *7* (9), 8233−8242.

DOI: 10.1021/acsami.9b15448
ACS Appl. Mater. Interfaces 2019, 11, 43223−43234